A tyrosine residue deprotonates during oxygen reduction by the caa3 reductase from *Rhodothermus marinus*

Manuela M. Pereira[a], Filipa L. Sousa[a], Miguel Teixeira[a], Rebecca M. Nyquist[b], Joachim Heberle[b,c,*]

[a] *Instituto de Tecnologia Química e Biológica, Universidade Nova de Lisboa Av. da República, Apartado 127, 2781-901 Oeiras, Portugal*
[b] *Forschungszentrum Jülich, IBI-2: Structural Biology, 52425 Jülich, Germany*
[c] *University of Bielefeld, Biophysical Chemistry, 33615 Bielefeld, Germany*

Abstract Heme-copper oxygen reductases catalyze proton translocation across the cellular membrane; this takes place during the reaction of oxygen to water. We demonstrate with attenuated total reflection-Fourier transform infrared (ATR-FTIR) difference spectroscopy that a tyrosine residue of the oxygen reductase from the thermohalophilic *Rhodothermus marinus* becomes deprotonated in the transition from the oxidized state to the catalytic intermediate ferryl state P_M. This tyrosine residue is most probably Y256, the helix VI tyrosine residue proposed to substitute for the D-channel glutamic acid that is absent in this enzyme. Comparison with the mitochondrial like oxygen reductase from *Rhodobacter sphaeroides* suggests that proton transfer from a strategically situated donor to the active site is a crucial step in the reaction mechanism of oxygen reductases.
© 2006 Federation of European Biochemical Societies. Published by Elsevier B.V. All rights reserved.

Keywords: FTIR; Vibrational spectroscopy; Cytochrome *c* oxidase; Respiration; Proton translocation; Electron transfer; Glutamic acid; Tyrosine; Membrane; Bacteriorhodopsin

1. Introduction

Oxygen reductases are the terminal complexes of aerobic respiratory chains, catalyzing the reduction of dioxygen to water. Most of these enzymes belong to the superfamily of heme copper oxygen reductases, which are characterized by the presence of a low-spin heme and a binuclear center that harbors a high-spin heme and a copper ion, capable of coupling oxygen reduction to proton translocation. These enzymes are able to oxidize peripheral or periplasmatic electron donors (such as cytochromes, high potential iron–sulfur proteins, or copper proteins) or membrane-bound electron donors (quinols). Upon reaction of the reduced enzyme with oxygen, several catalytic intermediates are formed, ultimately leading to complete reduction of oxygen to water. Some of these steps are coupled to proton translocation (Fig. 1A, green arrows) [1]. In the reductive phase (intermediates E and R), the input of two electrons reduces the binuclear center, enabling the bind-ing of dioxygen to the central iron of high spin heme. Both initial electron transfer reactions are coupled to net proton uptake by the protein. In the oxidative phase, bound dioxygen is cleaved and the high-spin heme is in the ferryl state with a bound oxygen atom ($Fe_{a3}^{4+} = O$, P state). The uptake of the third electron with a proton forms the F state, still a ferryl state. The final step (F to O) is driven by the uptake of the fourth electron. This intricate machinery will not be fully understood until the number of electrons and protons transferred at each reaction step within and across this proton pump is conclusively quantified and information at the single residue level as to when and where proton transfer steps take place is determined.

To perform their physiological function of reducing oxygen to water, and also to pump protons, proton pathways must exist (see D and K pathway in Fig. 1B). Based on the amino acid residues that form these channels, on amino acid sequence comparisons, and on specific characteristics of subunit II, three families have been established for heme copper oxygen reductases, named A (which includes the subfamilies A1 and A2), B, and C [2]. The *caa*3 oxygen reductase from the thermohalophilic *Rhodothermus (R.) marinus* is a typical member of type A2 subfamily of heme-copper oxygen reductases because it comprises all of the amino acid residues of the D- and K-channels as the mitochondrial-like type A1 heme-copper enzymes with the exception of the helix VI glutamic acid (E286 in *Rhodobacter sphaeroides* numbering). This residue is considered a key element for proton transfer; however, the *R. marinus* *caa*3 oxygen reductase has been shown to pump protons [3] despite this residue's absence. Based on a homology model for the *R. marinus* oxygen reductase and sequence comparison analysis [8], it has been suggested that a helix VI tyrosine residue (Fig. 1C), one helix turn below the position of E286 and whose hydroxyl group occupies the same spatial position as the terminal carboxylic acid of the type A1 enzymes (Fig. 1B), is involved in proton conduction [4].

We have shown by Fourier transform infrared (FTIR) spectroscopy that E286 acts as a proton shuttle in the oxygen reductase of *R. sphaeroides* because it is consecutively deprotonated and reprotonated twice within one catalytic turnover [5]. This finding has been challenged by FTIR experiments on the homologous enzyme from *Paracoccus denitrificans* [6] where only a change in H-bonding of the corresponding residue E278 has been reported for the P state. To further clarify this issue, we have chosen to examine the type A2 oxygen reductase, which lacks this critical residue. We demonstrate by

*Corresponding author. Fax: +49 0 521 1062981.
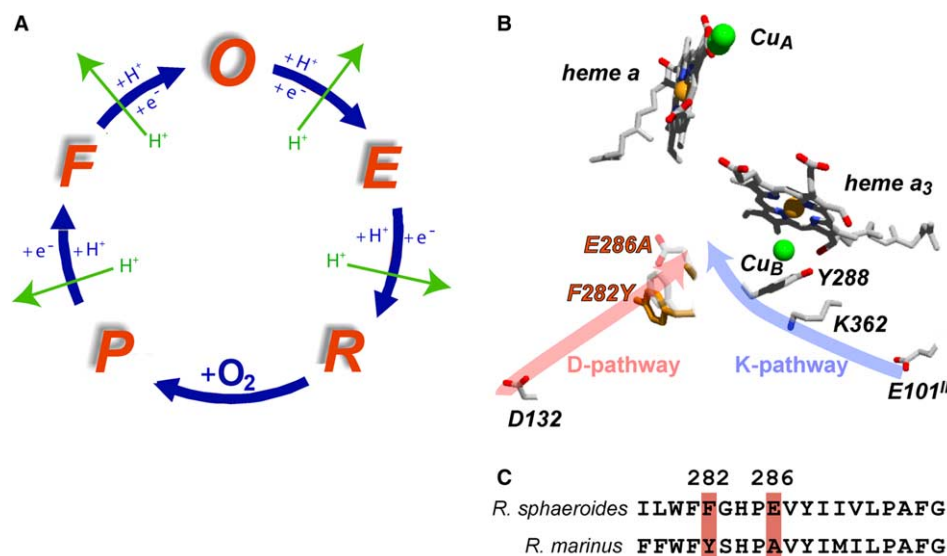E-mail address:* joachim.heberle@uni-bielefeld.de (J. Heberle).

Fig. 1. (A) Catalytic cycle of heme-copper oxygen reductases, adapted from [1]. The oxidized state (O) is sequentially reduced, and various intermediate states (E, R, P, and F) are formed. Four electrons and four protons are required to form H_2O from molecular O_2 (in blue). During turnover of the reductase, protons are translocated across the membrane (green arrows). (B) Structure of the *aa*3 oxygen reductase from *R. sphaeroides* (PDB entry: 1M56 [18]) with the proton uptake pathways D (due to D132) and K (due to K362). Glutamic acid 286 has been replaced by alanine (E286A) and phenylalanine 282 by a tyrosine residue (F282Y), which correspond to A260 and Y256 in the *caa*3 oxygen reductase from *R. marinus*. (C) Sequence alignment of subunit I of the *aa*3 oxidase from *R. sphaeroides* with subunit I from *R. marinus caa*3 oxidase. The relevant residue exchanges (F282 to Y, and E286 to A) are marked with red boxes.

FTIR spectroscopy that a tyrosine residue, most probably Y256, may substitute in the functional role of E286 by releasing a proton to the active site in the P state.

2. Materials and methods

Bacterial growth and membrane preparation and solubilization were performed as previously described in [7]. Protein purification followed the procedure reported in [8]. *R. marinus caa*3 oxygen reductase was reconstituted with dimyristoyl-phosphotidyl-choline and a film was prepared as described in [5,9]. Fully reduced samples were obtained by incubation with degassed solution of 50 mM potassium phosphate, 90 mM KCl, and 10 mM $Na_2S_2O_4$, pH 8.5. The P_M state was obtained by incubating the film with 50 mM potassium phosphate and 100 mM KCl, pH 8.5, saturated with equimolar amounts of CO and O_2. The F_H state was formed after incubation of the film with 50 mM potassium phosphate, 100 mM KCl and 1 mM H_2O_2, pH 8.5. For each intermediate state, the films were cycled between oxidized (with several washes of unsaturated buffer) and the respective intermediate state (with corresponding buffer described above). UV/Vis spectra were recorded on a Shimadzu UV-1603 or Olis DW2 spectrophotometer to validate the presence of each state.

FTIR experiments were performed on an IFS 66v spectrometer (Bruker, Rheinstetten, Germany) equipped with an attenuated total reflection (ATR) flow cell (Resultec, Garbsen, Germany). For each trapped reaction state, 5×5000 FTIR spectra at an optical resolution of $2 \ cm^{-1}$ were averaged (see [5,9] for further details). The spectroscopic differences after the reduction with dithionite were observed to be entirely reversible upon reoxidation by incubation with dithionite-free degassed buffer.

3. Results and discussion

3.1. Characterization of the reaction intermediates by UV/Vis spectroscopy

The visible difference spectra of the fully reduced minus oxidized *caa*3 oxygen reductase from *R. marinus* and *aa*3 oxygen reductase from *R. sphaeroides* are shown in Fig. 2 (black traces).

As previously described [8], the purified *caa*3 oxygen reductase from *R. marinus* presents Soret bands with maxima at 606 and 444 nm (characteristic of cytochrome *a*), and at 552 and 420 nm (characteristic of cytochrome *c*). Since the *caa*3 oxygen reductase from *R. marinus* has five redox centers, its fully reduced state is designated R_5 whereas that of the four-center *aa*3 oxygen reductase from *R. sphaeroides* is designated R_4.

We trapped the first stable oxygen intermediate P_M (the subscript M indicates that the P state is formed by reacting the mixed-valent state with oxygen [10]) upon incubation of the enzyme with CO/O_2, as confirmed by the presence of the peak at 607 nm in the visible difference spectrum ($P_M - O$ in Fig. 2, red trace, left panel). Under these conditions heme *a* remains oxidized while heme *a*3 becomes reduced and reacts with oxygen, yielding a ferryl state. In the Soret region, the maximum absorbance is observed at 448 nm. Although this wavelength is higher than that of the *R. sphaeroides* enzyme (Fig. 2, red trace, right panel), it is in the range of wavelength values where maximum absorbance is observed for the P_M state in several enzymes. Significant deviations between the $P_M - O$ difference spectra of the two enzymes are observed below 440 nm. This may be due to the presence of the additional heme (heme *c*) in the *R. marinus* enzyme. The P_M state of the *R. marinus* enzyme might differ in other aspects – evidence for such differences is needed from studies of the molecular nature of this state, e.g., by electron paramagnetic resonance or resonance Raman spectroscopy.

The subsequent state in the reaction cascade after oxygen splitting is the F state (Fig. 1A). The F state of *R. marinus caa*3 oxygen reductase was created by incubation with an excess of H_2O_2 (termed F_H). The UV/Vis difference spectrum between the F_H and O states (Fig. 2, green spectrum, left panel) exhibits a characteristic absorption at 579 nm, which is about the same wavelength as that of *R. sphaeroides aa*3 (Fig. 2, green spectrum, right panel). The difference band features in the Soret region are also identical to those of the well charac-
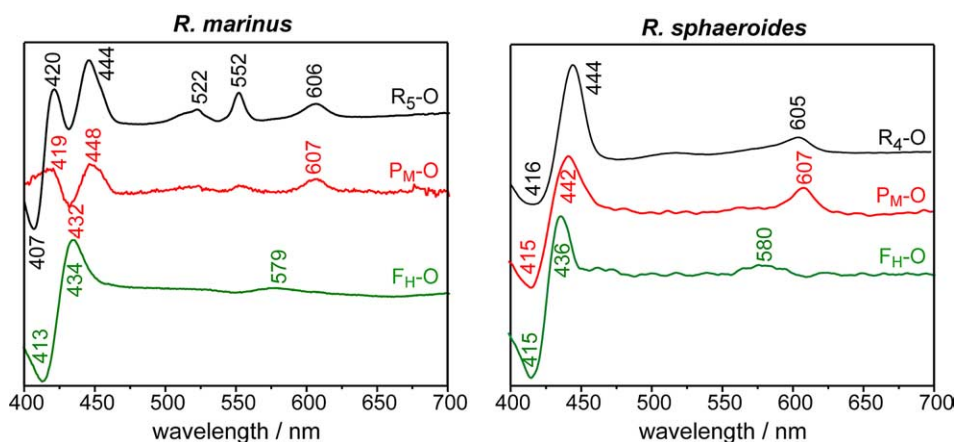
Fig. 2. UV/Vis difference spectra of the *caa*3 oxygen reductase from *R. marinus* and the *aa*3 oxygen reductase from *R. sphaeroides* in different oxidation states. Black traces: fully reduced minus oxidized ($R_5 - O$ and $R_4 - O$); red traces: P_M minus oxidized ($P_M - O$); green traces: F_H minus oxidized ($F_H - O$).

terized spectrum of *R. sphaeroides aa*3, providing evidence for the presence of the F_H state and indicating the presence of a heme *a*3 ferryl.

3.2. Characterization of the reaction intermediates by infrared difference spectroscopy

FTIR difference spectroscopy is highly sensitive towards structural changes that occur when the protein is transferred from one state to another. With the ATR technique [11], these state changes can be induced by perfusion, and differences on the level of a single vibration are monitored upon chemical conversion to the other state. The overall ATR-FTIR difference spectrum for fully reduced minus oxidized *caa*3 oxygen reductase (Fig. 3, top spectrum) presents difference bands similar to those of the other oxygen reductases, such as the *aa*3 oxygen reductase from *R. sphaeroides*, whose spectrum is shown for comparison (Fig. 3, bottom spectrum). Assignment of some of the features in the fully reduced minus oxidized difference spectra has been performed using the enzyme most closely related to the *R. marinus caa*3, the *caa*3 oxygen reductase from *Thermus thermophilus* [12]. Vibrational changes of the formyl side chain of heme *a*3 (C=O at 1664 cm^{-1}), the heme propionate (C=O at 1676 cm^{-1}), amide I (at 1632 cm^{-1}), and $v38y$ of heme *a* (at 1543 cm^{-1}) are present in the *R. marinus caa*3 spectrum. The positive peak at 1516 cm^{-1} and the negative band at

1501 cm^{-1} have also been assigned to a protonated tyrosine residue in the reduced state and a deprotonated tyrosine residue in the oxidized state, respectively [12]. This assignment is corroborated by the similarity of these difference bands to those of the tyrosinate minus tyrosine difference spectrum [5].

The ATR-FTIR difference spectra of the P_M minus oxidized *caa*3 oxygen reductase from *R. marinus* is shown in Fig. 4A (red spectrum). The spectrum strongly resembles the $P_M - O$ difference spectrum for the *aa*3 oxygen reductase from *R. sphaeroides* [5], shown in Fig. 4A (green spectrum) for comparison. Outside of the amide region (1600–1700 cm^{-1}), prominent bands are observed at 1516 (negative), 1498 (positive), 1361 (negative), and 1274 cm^{-1} (positive). By comparison with the pH-induced FTIR difference between the free
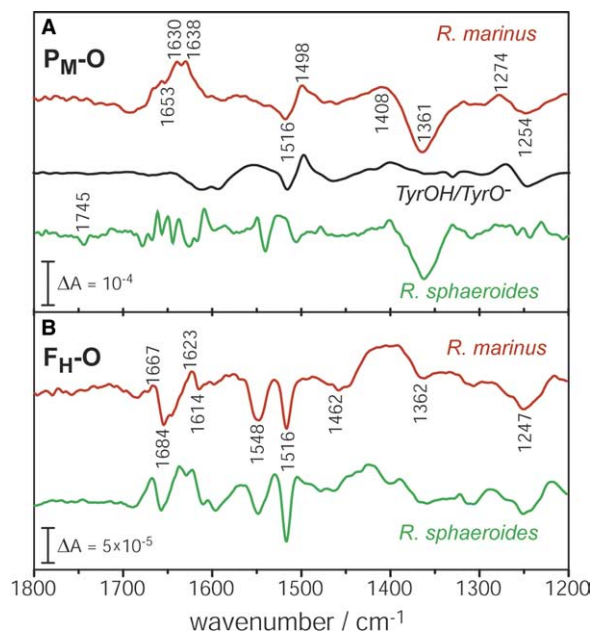
Fig. 4. FTIR absorption difference spectra of the oxygen intermediates of the *caa*3 oxygen reductase from *R. marinus* (red traces) and the *aa*3 oxygen reductase from *R. sphaeroides* (green traces). The bands that are indicated are discussed in the text. (A) $P_M - O$ difference spectra. For comparison, the pH-induced difference spectrum of the free amino acid tyrosine is shown (black trace). (B) $F_H - O$ difference spectra.
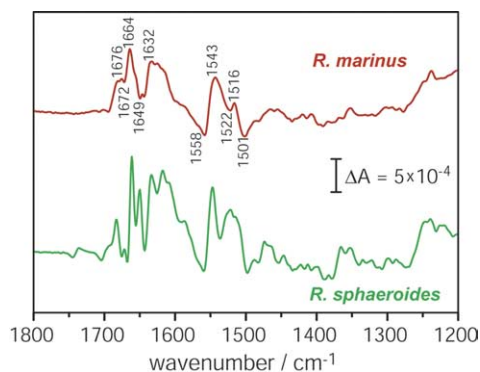

Fig. 3. ATR-FTIR difference spectra of the fully reduced minus oxidized *caa*3 oxygen reductase from *R. marinus* (top trace) and *aa*3 oxygen reductase from *R. sphaeroides* (bottom trace).

amino acid tyrosine and the corresponding base, tyrosinate (Fig. 4A, black spectrum), the negative band at 1516 cm^{-1} is assigned to the phenyl ring stretching mode of tyrosine that downshifts to 1498 cm^{-1} (positive) upon formation of the tyrosinate. Correspondingly, the C–O–H vibration (C–O stretch coupled to O–H bend) of the phenolic ring moves from 1254 (negative) to 1274 cm^{-1} (positive). The frequencies and the spectral shifts provide strong evidence for the deprotonation of a tyrosine side chain in the P_M state. The prominent trough at 1361 cm^{-1} may reflect the heme $a3$ ferric to ferryl conversion as discussed in [13], corroborating the visible data (Fig. 2) that confirm formation of the P_M state.

The most natural candidate for a tyrosine residue of the *R. marinus caa*3 oxygen reductase that could exhibit such behavior is Y256. The side chain of this amino acid residue occupies nearly the same location as the equivalent E286 of the *R. sphaeroides aa*3 oxygen reductase (Fig. 1B). Indeed, the P_M − O difference spectrum of the latter exhibits a negative band at 1745 cm^{-1} that has previously been assigned to the C=O stretching vibration of E286 [5] (Fig. 4A, green spectrum). The negative band is evidence for E286 deprotonated in the P_M state of the *R. sphaeroides* enzyme. Since this glutamic acid is replaced by an alanine in the amino acid sequence of the *R. marinus* oxygen reductase, no difference band should appear in the C=O stretching region. This is indeed the case, experimentally verified by an essentially flat line at frequencies above 1700 cm^{-1} (red spectrum in Fig. 4A). Thus, we conclude that a tyrosine residue, most probably Y256, from *R. marinus caa*3 plays the same role as E286 from *R. sphaeroides aa*3, i.e. donating a proton to the active site during the lifetime of the P_M state. A definitive assignment to Y256 can only be made via experiments with site-directed mutants of the *R. marinus caa*3. However, a conservative mutant would be needed, and critical tyrosines in particular, most often cannot be conservatively replaced without annihilating the redox activity of the oxygen reductase [14].

The ATR-FTIR difference spectra of F_H − O *caa*3 oxygen reductase from *R. marinus* is shown in Fig. 4B (red spectrum). This difference spectrum is very similar to that of the *R. sphaeroides* enzyme (green spectrum in Fig. 4B and [5]) as well as that of the *P. denitrificans* enzyme [13]. Prominent vibrational bands at 1548 and 1516 cm^{-1} are observed for the *R. marinus* oxygen reductase (red spectrum). These bands have been assigned to the deprotonated state of the covalently linked tyrosine [5]. In comparison to the spectrum of the *R. spharoides* oxygen reductase, the trough at 1516 cm^{-1} in the *R. marinus* spectrum is less pronounced. This may indicate the protonation of another tyrosine residue whose vibrational bands would partially compensate the band assigned to the deprotonation of the covalently linked tyrosine. The spectral features in the 1600–1700 cm^{-1} region as well as the negative bands at 1462 and 1362 cm^{-1} are almost identical for the *R. marinus* and *R. sphaeroides* enzymes. Expected in this region are formyl and porphyrin ring modes that are sensitive to the redox and ligation states of the heme iron [15,16] and reflect the heme $a3$ ferric to ferryl conversion [13]. The differences in the amide I region are most likely due to small changes in the protein backbone, and not to changes at the redox centers. Due to the low overall amino acid sequence identity between *R. marinus caa*3 and *R. sphaeroides aa*3 oxygen reductase, amide I differences are expected. Overall, the close similarity of the F_H − O difference spectra of the oxygen reductases from

R. marinus and *R. sphaeroides* demonstrates that both enzymes undergo fundamentally the same reaction mechanism. Therefore, it is highly probable that the deprotonation of a residue close to the binuclear center is an essential step in the formation of the P_M state in all oxygen reductases.

4. Conclusions

This work shows that the operational themes of the catalytic centers in types A1 and A2 oxygen reductases [2] are the same, and that equivalent protonation events are present although they are performed by different amino acid residues. It is evident that a proton is transferred from a strategically placed proton donor (either a glutamic acid, as in type A1 oxygen reductases, or a tyrosine residue, as in type A2 oxygen reductases) to the active site during the lifetime of the P_M state. This result contradicts many theoretical models (see [17] for an overview) that propose a gating mechanism which relies solely on the reorientation of the glutamic acid and the surrounding water molecules without requiring an actual deprotonation reaction. Most importantly, knowledge of the charge state of residues is crucial for gaining further mechanistic insight because proton relocation during enzymatic catalysis is the most efficient way to alter the electrostatics in a protein.

References

[1] Bloch, D., Belevich, I., Jasaitis, A., Ribacka, C., Puustinen, A., Verkhovsky, M.I. and Wikström, M. (2004) The catalytic cycle of cytochrome *c* oxidase is not the sum of its two halves. Proc. Natl. Acad. Sci. USA 101, 529–533.

[2] Pereira, M.M. and Teixeira, M. (2004) Proton pathways, ligand binding and dynamics of the catalytic site in haem-copper oxygen reductases: a comparison between the three families. Biochim. Biophys. Acta 1655, 340–346.

[3] Pereira, M.M., Verkhovskaya, M.L., Teixeira, M. and Verkhovsky, M.I. (2000) The caa(3) terminal oxidase of Rhodothermus marinus lacking the key glutamate of the D-channel is a proton pump. Biochemistry 39, 6336–6340.

[4] Soares, C.M., Baptista, A.M., Pereira, M.M. and Teixeira, M. (2004) Investigation of protonatable residues in *Rhodothermus marinus* caa3 haem-copper oxygen reductase: comparison with *Paracoccus denitrificans* aa3 haem-copper oxygen reductase. J. Biol. Inorg. Chem. 9, 124–134.

[5] Nyquist, R.M., Heitbrink, D., Bolwien, C., Gennis, R.B. and Heberle, J. (2003) Direct observation of protonation reactions during the catalytic cycle of cytochrome *c* oxidase. Proc. Natl. Acad. Sci. USA 100, 8715–8720.

[6] Iwaki, M., Puustinen, A., Wikstrom, M. and Rich, P.R. (2004) ATR-FTIR spectroscopy and isotope labeling of the PM intermediate of *Paracoccus denitrificans* cytochrome *c* oxidase. Biochemistry 43, 14370–14378.

[7] Pereira, M.M., Carita, J.N. and Teixeira, M. (1999) Membrane-bound electron transfer chain of the thermohalophilic bacterium *Rhodothermus marinus*: a novel multihemic cytochrome *bc*, a new complex III. Biochemistry 38, 1268–1275.

[8] Pereira, M.M., Santana, M., Soares, C.M., Mendes, J., Carita, J.N., Fernandes, A.S., Saraste, M., Carrondo, M.A. and Teixeira, M. (1999) The caa3 terminal oxidase of the thermohalophilic bacterium *Rhodothermus marinus*: a HiPIP:oxygen oxidoreductase lacking the key glutamate of the D-channel. Biochim. Biophys. Acta 1413, 1–13.

[9] Nyquist, R.M., Heitbrink, D., Bolwien, C., Wells, T.A., Gennis, R.B. and Heberle, J. (2001) Perfusion-induced redox differences in cytochrome *c* oxidase: ATR/FT-IR spectroscopy. FEBS Lett. 505, 63–67.

[10] Nicholls, P. and Chanady, G.A. (1981) Interactions of cytochrome aa3 with oxygen and carbon monoxide. The role of the 607 nm complex. Biochim. Biophys. Acta 634, 256–265.

[11] Nyquist, R.M., Ataka, K. and Heberle, J. (2004) The molecular mechanism of membrane proteins probed by evanescent infrared waves. Chembiochem 5, 431–436.

[12] Hellwig, P., Pfitzner, U., Behr, J., Rost, B., Pesavento, R.P., Donk, W.V., Gennis, R.B., Michel, H., Ludwig, B. and Mäntele, W. (2002) Vibrational modes of tyrosines in cytochrome *c* oxidase from *Paracoccus denitrificans*: FTIR and electrochemical studies on Tyr-D4-labeled and on Tyr280His and Tyr35-Phe mutant enzymes. Biochemistry 41, 9116–9125.

[13] Iwaki, M., Puustinen, A., Wikström, M. and Rich, P.R. (2003) ATR-FTIR spectroscopy of the P(M) and F intermediates of bovine and *Paracoccus denitrificans* cytochrome *c* oxidase. Biochemistry 42, 8809–8817.

[14] Budiman, K., Kannt, A., Lyubenova, S., Richter, O.M., Ludwig, B., Michel, H. and MacMillan, F. (2004) Tyrosine 167: the origin of the radical species observed in the reaction of cytochrome *c* oxidase with hydrogen peroxide in *Paracoccus denitrificans*. Biochemistry 43, 11709–11716.

[15] Behr, J., Michel, H., Mäntele, W. and Hellwig, P. (2000) Functional properties of the heme propionates in cytochrome *c* oxidase from *Paracoccus denitrificans*. Evidence from FTIR difference spectroscopy and site-directed mutagenesis. Biochemistry 39, 1356–1363.

[16] Heibel, G.E., Hildebrandt, P., Ludwig, B., Steinrucke, P., Soulimane, T. and Buse, G. (1993) Comparative resonance Raman study of cytochrome *c* oxidase from beef heart and *Paracoccus denitrificans*. Biochemistry 32, 10866–10877.

[17] Olsson, M.H., Sharma, P.K. and Warshel, A. (2005) Simulating redox coupled proton transfer in cytochrome *c* oxidase: looking for the proton bottleneck. FEBS Lett. 579, 2026–2034.

[18] Svensson-Ek, M., Abramson, J., Larsson, G., Tornroth, S., Brzezinski, P. and Iwata, S. (2002) The X-ray crystal structures of wild-type and EQ(I-286) mutant cytochrome *c* oxidases from *Rhodobacter sphaeroides*. J. Mol. Biol. 321, 329–339.